

Frozen natural spinors for Cholesky decomposition based two-component relativistic coupled cluster method.

Somesh Chamoli,[†] Xubo Wang,[‡] Chaoqun Zhang,[¶] Malaya K. Nayak,[§] and Achintya Kumar Dutta^{*,†}

[†]*Department of Chemistry, Indian Institute of Technology Bombay, Powai, Mumbai 400076, India*

[‡]*Department of Chemistry, the Johns Hopkins University, Baltimore, Maryland 21218, United States*

[¶]*Department of Chemistry, Yale University, New Haven, Connecticut 06520, United States*

[§]*Theoretical Chemistry Section, Bhabha Atomic Research Centre, Trombay, Mumbai 400085, India*

E-mail: achintya@chem.iitb.ac.in

Abstract

We present an efficient and cost-effective implementation for the exact two-component atomic mean field (X2CAMF)-based coupled cluster (CC) method, which integrates frozen natural spinors (FNS) and the Cholesky decomposition (CD) technique. The use of CD approximation greatly reduces the storage requirement of the calculation without any significant reduction in accuracy. Compared to four-component methods, the FNS and CD-based X2CAMF-CC approach gives similar accuracy as that of the canonical four-component relativistic coupled cluster method at a fraction of the cost. The efficiency of the method is demonstrated by the calculation of a medium-sized uranium complex involving the correlation of over 1000 virtual spinors.

1 Introduction

Reliable predictions of molecular properties for molecules containing heavy elements require accurate treatment of both relativistic effects and electron correlation. The coupled cluster (CC) methods utilizing relativistic four-component or two-component Hamiltonians have proven to be effective approaches for achieving high accuracy in quantum chemistry simulations involving such molecules.¹⁻⁷ The four-component relativistic coupled cluster (CC) methods, based on the Dirac-Coulomb(-Breit) Hamiltonian, are among the most accurate relativistic CC techniques available; however, they are also the most computationally expensive. The transformation and storage of two-electron integrals in the molecular spinor basis have limited the use of four-component CC methods to relatively small molecular systems.

To alleviate the high computational cost associated with four-component methods, various two-component theories⁸⁻¹⁴ have been introduced. Among these, the exact two-component (X2C) theory^{10,13,15-17} has gained recognition as a particularly prominent approach, which can reduce the computational cost of the integral transformation step. The literature covers a diverse array of X2C-CC methods, each providing various approaches and enhancements suited to different applications and computational requirements. This includes the spin-free (SF) version of X2C-CC theory in its mean-field form (the SFX2C-mf scheme),¹⁸ the SFX2C-CC theory in its one-electron form (the SFX2C-1e scheme),¹⁹⁻²¹ and the X2C molecular mean field (X2CMMF) based CC method.²²⁻²⁶ Among various X2C-CC methods, the X2C-CC approach that uses atomic mean field (AMF)²⁷ spin-orbit (SO) integrals referred to as the X2CAMF-CC scheme²⁸⁻³⁰ has emerged as an attractive option to perform highly accurate relativistic coupled cluster calculation. By integrating atomic mean-field spin-orbit effects into the X2C theory, the X2CAMF method delivers a comprehensive treatment of both spin-orbit and scalar-relativistic effects while enhancing computational efficiency and maintaining accuracy for CC calculations, making it particularly suitable for systems involving heavy elements.

Although the X2CAMF-CC scheme provides a computational advantage over the four-component and X2CMMF methods, its application to large or medium-sized molecules remains limited due to the substantial storage required for two-electron integrals. Furthermore, the inherently high computational cost of the coupled cluster method itself restricts its applicability. For instance, the widely used coupled cluster singles-doubles (CCSD) method scales computationally as $O(N^6)$ with respect to the size of the basis set. Various approaches, such as density-fitting (DF)^{31,32} and Cholesky decomposition (CD),³³⁻³⁵ have been employed to reduce the computational cost of relativistic calculations by decomposing the two-electron integrals thereby reducing both disk-space and memory demands. A CD-based X2CAMF-CC and equation of motion (EOM) CC method has also been recently introduced to address storage limitations, enabling calculations for medium-sized molecules.³⁶

Despite the advantage of significantly optimized disk and memory requirements, CD-based X2CAMF-CC implementations still involve a similar number of floating-point operations as conventional X2CAMF-CC techniques. Thus, it is crucial to minimize the floating-point operations to make CD-based X2CAMF-CC methods applicable to larger molecules and extend their scope of usefulness. To accelerate floating-point operations, one can utilize massively parallel programs designed to scale across multiple cores.^{24,37,38} Alternatively, one can reduce the floating-point operations required in CC calculations by using natural spinors. Natural spinors, the relativistic analog of natural orbitals,³⁹ offer a more compact description of orbital space and can substantially lower the computational cost of relativistic CD-based X2CAMF-CC calculations. An implementation of frozen natural spinors within both the four-component⁴⁰⁻⁴² and two-component⁴³ frameworks already exists in the literature to reduce the computational cost of relativistic CC and EOM-CC calculations. This paper aims to combine the frozen natural spinor framework and the CD-based X2CAMF-CCSD and CCSD(T) methods to simultaneously reduce storage requirements as well as floating-point operations. The present implementation of the CD-X2CAMF-CC method allows one to routinely perform coupled cluster calculations for systems with more than 1000 spinors in a

single computing node.

2 Theory

2.1 Exact two-component Hamiltonian with atomic mean field integrals (the X2CAMF scheme)

The X2CAMF scheme generates the two-component Hamiltonian by transforming the original four-component Dirac-Coulomb (DC) Hamiltonian using the X2C decoupling approach.¹⁰

The four-component DC Hamiltonian can be expressed as

$$\hat{H}^{4c} = \sum_{pq} h_{pq}^{4c} a_p^\dagger a_q + \frac{1}{4} \sum_{pqrs} g_{pqrs}^{4c} a_p^\dagger a_q^\dagger a_s a_r \quad (1)$$

Here, the summation is restricted to positive-energy spinors only, in accordance with the no-pair approximation,⁴⁴ and the indices p, q, r, s denote positive-energy four-component spinors. Within the spin-separation scheme,⁴⁵ the antisymmetrized two-electron integrals can be split into their spin-free (SF) and spin-dependent (SD) parts

$$g_{pqrs}^{4c} = g_{pqrs}^{4c,SF} + g_{pqrs}^{4c,SD} \quad (2)$$

Using Eq. (2) in Eq. (1) the four-component DC Hamiltonian becomes

$$\hat{H}^{4c} = \sum_{pq} h_{pq}^{4c} a_p^\dagger a_q + \frac{1}{4} \sum_{pqrs} g_{pqrs}^{4c,SD} a_p^\dagger a_q^\dagger a_s a_r + \frac{1}{4} \sum_{pqrs} g_{pqrs}^{4c,SF} a_p^\dagger a_q^\dagger a_s a_r \quad (3)$$

Utilizing the local nature of the spin-orbit interaction, the spin-dependent component of the Coulomb interaction in the four-component DC Hamiltonian can be handled using the

atomic mean-field (AMF) approximation.²⁷

$$\frac{1}{4} \sum_{pqrs} g_{pqrs}^{4c,SD} a_p^\dagger a_q^\dagger a_s a_r \approx \sum_{pq} g_{pq}^{4c,AMF} a_p^\dagger a_q = \sum_{pq} \sum_A \sum_i n_{iA} g_{pi_Aqi_A}^{4c,SD} a_p^\dagger a_q \quad (4)$$

Here, A represents the distinct atoms in the molecule, with the index i denoting the occupied spinors for atom A , and n_{iA} signifies their corresponding occupation numbers. Therefore, the Hamiltonian becomes

$$\hat{H}^{4c} = \sum_{pq} h_{pq}^{4c} a_p^\dagger a_q + \sum_{pq} g_{pq}^{4c,AMF} a_p^\dagger a_q + \frac{1}{4} \sum_{pqrs} g_{pqrs}^{4c,SF} a_p^\dagger a_q^\dagger a_s a_r \quad (5)$$

Now, the above Hamiltonian can be transformed into a two-component representation. In Eq. (5), the first term h_{pq}^{4c} , which has a form of

$$h^{4c} = \begin{pmatrix} V & T \\ T & \frac{1}{4m^2c^2}W - T \end{pmatrix} \quad (6)$$

with V as a nuclear potential matrix, T as a kinetic energy matrix, and $W = (\boldsymbol{\sigma} \cdot \mathbf{p})V(\boldsymbol{\sigma} \cdot \mathbf{p})$ as small components nuclear attraction matrix, where $\boldsymbol{\sigma}$ being Pauli spin matrices and \mathbf{p} is the momentum operator, will transform into

$$h^{X2C} = R^\dagger [V + X^\dagger T + TX + X^\dagger (\frac{1}{4m^2c^2}W - T)X] R \quad (7)$$

In Eq. (7), the X matrix links the coefficients of the large and small component wavefunctions, while the R matrix connects the coefficients of the large component wavefunction to the two-component wavefunction.

$$C^S = XC^L \quad (8)$$

$$C^L = RC^{2c} \quad (9)$$

For the second term in Eq. (5), a transformation of four-component AMF integrals into a two-component picture will be carried out for each atom using the same X and R matrices. After transformation $g_{pq}^{4c,AMF}$ takes the form of $g_{pq}^{2c,AMF}$. For the third term in Eq. (5), which represents a scalar two-electron contribution, if errors from the change of picture can be ignored, it simplifies to the nonrelativistic two-electron integrals after transformation.

$$g_{pqrs}^{4c,SF} \approx g_{pqrs}^{NR} \quad (10)$$

Thus, after transforming into a two-component representation, the overall Hamiltonian becomes

$$\hat{H}^{X2CAMF} = \sum_{pq} h_{pq}^{X2C} a_p^\dagger a_q + \sum_{pq} g_{pq}^{2c,AMF} a_p^\dagger a_q + \frac{1}{4} \sum_{pqrs} g_{pqrs}^{NR} a_p^\dagger a_q^\dagger a_s a_r \quad (11)$$

The above X2CAMF Hamiltonian can be expressed as an effective one-electron operator combined with a nonrelativistic two-electron operator, as follows:

$$\hat{H}^{X2CAMF} = \sum_{pq} h_{pq}^{X2CAMF} a_p^\dagger a_q + \frac{1}{4} \sum_{pqrs} g_{pqrs}^{NR} a_p^\dagger a_q^\dagger a_s a_r \quad (12)$$

with

$$h^{X2CAMF} = h^{X2C} + g^{2c,AMF} \quad (13)$$

The primary benefit of using the X2CAMF Hamiltonian is that it avoids the formation of molecular relativistic two-electron integrals.

2.2 Relativistic coupled cluster method

The foundation of CC theory⁴⁶ lies in the exponential parametrization of the wavefunction

$$|\Psi_{cc}\rangle = e^{\hat{T}}|\Phi_0\rangle, \quad (14)$$

where $|\Phi_0\rangle$ denotes the reference determinant, and \hat{T} is the cluster excitation operator with its form as

$$\hat{T} = \hat{T}_1 + \hat{T}_2 + \cdots + \hat{T}_N, \quad (15)$$

where any general n-tuple excitation operator can be represented as

$$\hat{T}_n = \left(\frac{1}{n!}\right)^2 \sum_{ij\dots ab\dots} t_{ij\dots}^{ab\dots} a_a^\dagger a_b^\dagger \dots a_j a_i \dots \quad (16)$$

In Eq. (16), $t_{ij\dots}^{ab\dots}$ denote the cluster amplitudes. The indices $(i, j, k \dots)$ represent occupied spinors, while $(a, b, c \dots)$ indicate virtual spinors. By limiting the cluster operator to include only one-body (\hat{T}_1) and two-body (\hat{T}_2) excitations, one arrives at the widely used CCSD approximation.

$$\hat{T} = \hat{T}_1 + \hat{T}_2 = \sum_{ia} t_i^a a_a^\dagger a_i + \frac{1}{4} \sum_{ijab} t_{ij}^{ab} a_a^\dagger a_b^\dagger a_j a_i \quad (17)$$

To obtain the cluster amplitudes (t_i^a , and t_{ij}^{ab}), one needs to solve a system of non-linear equations simultaneously

$$\langle \Phi_i^a | \bar{H} | \Phi_0 \rangle = 0, \quad (18)$$

$$\langle \Phi_{ij}^{ab} | \bar{H} | \Phi_0 \rangle = 0, \quad (19)$$

where $|\Phi_i^a\rangle$ and $|\Phi_{ij}^{ab}\rangle$ are the excited determinants and $\bar{H} = e^{-\hat{T}} \hat{H}^{X2CAMF} e^{\hat{T}}$ is the similarity transformed Hamiltonian, with \hat{H}^{X2CAMF} is defined in Eq. (12). The CCSD ground state energy is determined by the expression

$$\langle \Phi_0 | \bar{H} | \Phi_0 \rangle = E, \quad (20)$$

The CCSD(T) method strikes an ideal balance between computational efficiency and accuracy, addressing the limitations of the CCSD method in achieving quantitative precision. In CCSD(T), the triples correction to energy is determined non-iteratively based on the amplitudes from the converged CCSD calculation.

$$E_{(T)} = \frac{1}{36} \sum_{ijk} \sum_{abc} [t(c)_{ijk}^{abc} + t(d)_{ijk}^{abc}] D_{ijk}^{abc} t(c)_{ijk}^{abc}, \quad (21)$$

with $t(c)_{ijk}^{abc}$ and $t(d)_{ijk}^{abc}$ as connected and disconnected triple amplitudes defined by:

$$D_{ijk}^{abc} t(c)_{ijk}^{abc} = P(ij/k)P(ab/c) \left[\sum_e t_{ij}^{ae} \langle bc || ek \rangle - \sum_m t_{im}^{ab} \langle mc || jk \rangle \right], \quad (22)$$

and

$$D_{ijk}^{abc} t(d)_{ijk}^{abc} = P(ij/k)P(ab/c) [t_k^c \langle ab || ij \rangle + t_{ij}^{ab} f_{kc}], \quad (23)$$

where

$$D_{ijk}^{abc} = f_{ii} + f_{jj} + f_{kk} - f_{aa} - f_{bb} - f_{cc}, \quad (24)$$

and P is the three-index permutation operator whose action on any arbitrary function ϕ is defined as

$$P(pq/r)\phi(pqr) = \phi(pqr) - \phi(rqp) - \phi(prq), \quad (25)$$

2.3 Cholesky decomposition

In Cholesky decomposition (CD),⁴⁷ any symmetric positive semi-definite matrix (M) can be approximated as

$$M \approx LL^T, \quad (26)$$

where L is a lower (or upper) triangular matrix referred to as the Cholesky vectors. This concept can be extended to positive semi-definite electron repulsion integrals (ERIs)

$$(\mu\nu|k\lambda) \approx \sum_P^{n_{CD}} L_{\mu\nu}^P L_{k\lambda}^P, \quad (27)$$

with μ, ν, k, λ as AO indices, $L_{\mu\nu}^P$ denoting the Cholesky vectors and n_{CD} being the total number of Cholesky vectors. These vectors are generated iteratively by identifying the largest diagonal elements of the ERI matrix $(\mu\nu|\mu\nu)$, and the process continues until the largest diagonal element falls below the predefined Cholesky threshold (τ).

The Cholesky vectors in the AO basis can be transformed to the MO basis as follows.

$$L_{pq}^P = \sum_{\mu\nu} C_{\mu p}^* L_{\mu\nu}^P C_{\nu q}, \quad (28)$$

These transformed vectors can then be used to generate antisymmetrized two-electron inte-

grals on the fly in the MO basis.

$$\langle pq||rs\rangle = \sum_P^{n_{CD}} (L_{pr}^P L_{qs}^P - L_{ps}^P L_{qr}^P), \quad (29)$$

In the current implementation, we avoid constructing and storing integrals of the form $\langle ab||cd\rangle$ and $\langle ab||ci\rangle$, instead generating them on the fly as needed. However, integrals with two or fewer virtual indices are explicitly constructed.

2.4 Frozen natural spinors

Natural spinors are derived from the correlated one-body reduced density matrix (1-RDM), which is constructed from a spin-orbit-coupled wavefunction obtained from a relativistic electron correlation calculation.⁴⁰ The eigenfunctions obtained from the diagonalization of this correlated 1-RDM are called natural spinors. They can be identified as the relativistic counterparts of Löwdin’s natural orbitals.³⁹ The Natural spinors framework is a useful tool for comprehending important spin-dependent phenomena within the confines of the relativistic environment. For instance, natural spinors have the ability to accurately mimic the spin-orbit splitting observed in subshells.⁴⁸ In addition, the use of natural spinors can offer insights into the significance of spin-orbit coupling in covalent bonding, as well as aid in the comprehension of the Jahn-Teller effect.^{49,50} There is an abundance of research on approaches that utilize natural orbitals for the decrease of computational expenses in non-relativistic correlation calculations.^{51–66} The favorable scaling of MP2 method makes it a popular choice for generating natural orbitals in non-relativistic ground-state coupled cluster calculations. In four-component relativistic methods, the generation of natural spinors for the reduction of computational cost under the no-pair approximation is achieved by utilizing a similar methodology of MP2 theory in the nonrelativistic domain.^{40–43}

To obtain MP2-based natural spinors, one can follow the following steps in sequence:

First, the virtual-virtual block of the 1-RDM (D_{ab}) is constructed using the MP2 method.

$$D_{ab} = \sum_{cij} \frac{\langle ac||ij\rangle \langle ij||bc\rangle}{\varepsilon_{ij}^{ac} \varepsilon_{ij}^{bc}} \quad (30)$$

Here,

$$\varepsilon_{ij}^{ac} = \varepsilon_i + \varepsilon_j - \varepsilon_a - \varepsilon_c \quad (31)$$

$$\varepsilon_{ij}^{bc} = \varepsilon_i + \varepsilon_j - \varepsilon_b - \varepsilon_c \quad (32)$$

In Eq. (31) and (32), ε_i , ε_j , ε_a , ε_b , and ε_c are molecular spinor energies, and $\langle ac||ij\rangle$ and $\langle ij||bc\rangle$ denotes the antisymmetrized two-electron integrals. The next step is the diagonalization of D_{ab} .

$$D_{ab}V = Vn \quad (33)$$

The eigenvectors (V) obtained in Eq. (33) are called virtual natural spinors, and the corresponding eigenvalues (n) are known as occupation numbers. The virtual natural spinors can be categorized based on their relevance to the overall correlation energy by utilizing their respective occupation numbers. By setting a predetermined threshold or cutoff for the occupation numbers of virtual natural spinors, the virtual space can be shortened by retaining only those spinors that meet or exceed this threshold. The subsequent step involves converting the virtual-virtual block of the Fock matrix into the truncated basis of natural spinors.

$$F_{vv}^{NS} = \tilde{V}^\dagger F_{vv} \tilde{V} \quad (34)$$

Here, \tilde{V} are virtual natural spinors in a truncated basis. F_{vv} represents a virtual-virtual

block of the initial canonical Fock matrix, and F_{vv}^{NS} is the virtual-virtual block of the Fock matrix in a truncated virtual natural spinor basis. Afterward, the F_{vv}^{NS} block is diagonalized in the natural spinor basis to obtain the semi-canonical virtual natural spinors (\tilde{Z}) and their associated orbital energies (ϵ).

$$F_{vv}^{NS} \tilde{Z} = \tilde{Z} \epsilon \quad (35)$$

A transformation matrix (U) can be constructed with the help of \tilde{V} and \tilde{Z} , which can be used to convert the canonical virtual spinor space to the semi-canonical natural virtual spinor space.

$$U = \tilde{Z} \tilde{V} \quad (36)$$

The occupied spinors within our chosen basis are kept in their canonical form, while the virtual spinors undergo a transformation to become semi-canonical natural virtual spinors. Hence, the process is also known as the “frozen natural spinors (FNS) method”. Using this FNS basis, it is now feasible to conduct higher-order correlation calculations (such as CCSD/CCSD(T)) at low computational costs. Coupled cluster methods that utilize natural orbitals in the non-relativistic realm have seen a significant improvement in accuracy by means of perturbative corrections.^{55,57} Similar is the case found in the four-component relativistic coupled cluster method based on frozen natural spinors.⁴⁰ By utilizing the ΔE_{MP2} approximation for $\Delta E_{CCSD/CCSD(T)}$, it is possible to apply a perturbative correction for the truncated virtual space.

$$\Delta E_{CCSD/CCSD(T)} = E_{CCSD/CCSD(T)}^{Canonical} - E_{CCSD/CCSD(T)}^{FNS} \quad (37)$$

$$\Delta E_{CCSD/CCSD(T)} \approx \Delta E_{MP2} \quad (38)$$

with

$$\Delta E_{MP2} = E_{MP2}^{Canonical} - E_{MP2}^{FNS} \quad (39)$$

3 Implementation and Computational Details

The FNS-CD-X2CAMF-CCSD/CCSD(T) method has been implemented in the development version of BAGH.⁶⁷ The X2CAMF DHF calculations are performed using the socutils package⁶⁸ interfaced with BAGH. Additionally, only the LOO and LOV-type 3 center two-electron integrals are created in the canonical molecular spinor basis; LVV-type Cholesky vectors are formed directly in the FNS basis, where O and V denote occupied and virtual spinors, respectively. It significantly accelerates the integral transformation phase and dramatically minimizes the storage requirement. Figure 1 presents a schematic depiction of the steps involved in the FNS-CD-X2CAMF-CCSD/CCSD(T) method

The first step comprises the solution of the X2CAMF-HF method. Next, the Cholesky vectors are produced in the AO basis. The next step is to generate LOO and LOV-type Cholesky vectors in a canonical MO basis (using Eq. (28)), which is necessary for the MP2 calculations. This step is followed by the construction of 1-RDM using MP2 amplitudes and diagonalization of 1-RDM to form natural spinors. After that, a transformation matrix is generated using Eq. (36) and its contraction with the original coefficient matrix to transform the AO basis directly to the FNS basis. The next step is the formation of LVV and LOV-type Cholesky vectors and antisymmetrized 0-2 particle (external) integrals using them in the FNS basis through the transformation matrix. Any construction or storage of four-particle or three-particle one-hole integrals is completely avoided and is generated on the fly using Cholesky vectors in the FNS basis. Now, these transformed integrals can be used for any higher-level correlation calculations, such as CCSD and CCSD(T).

To evaluate the performance of the FNS-CD-X2CAMF-CCSD/CCSD(T) method, a com-

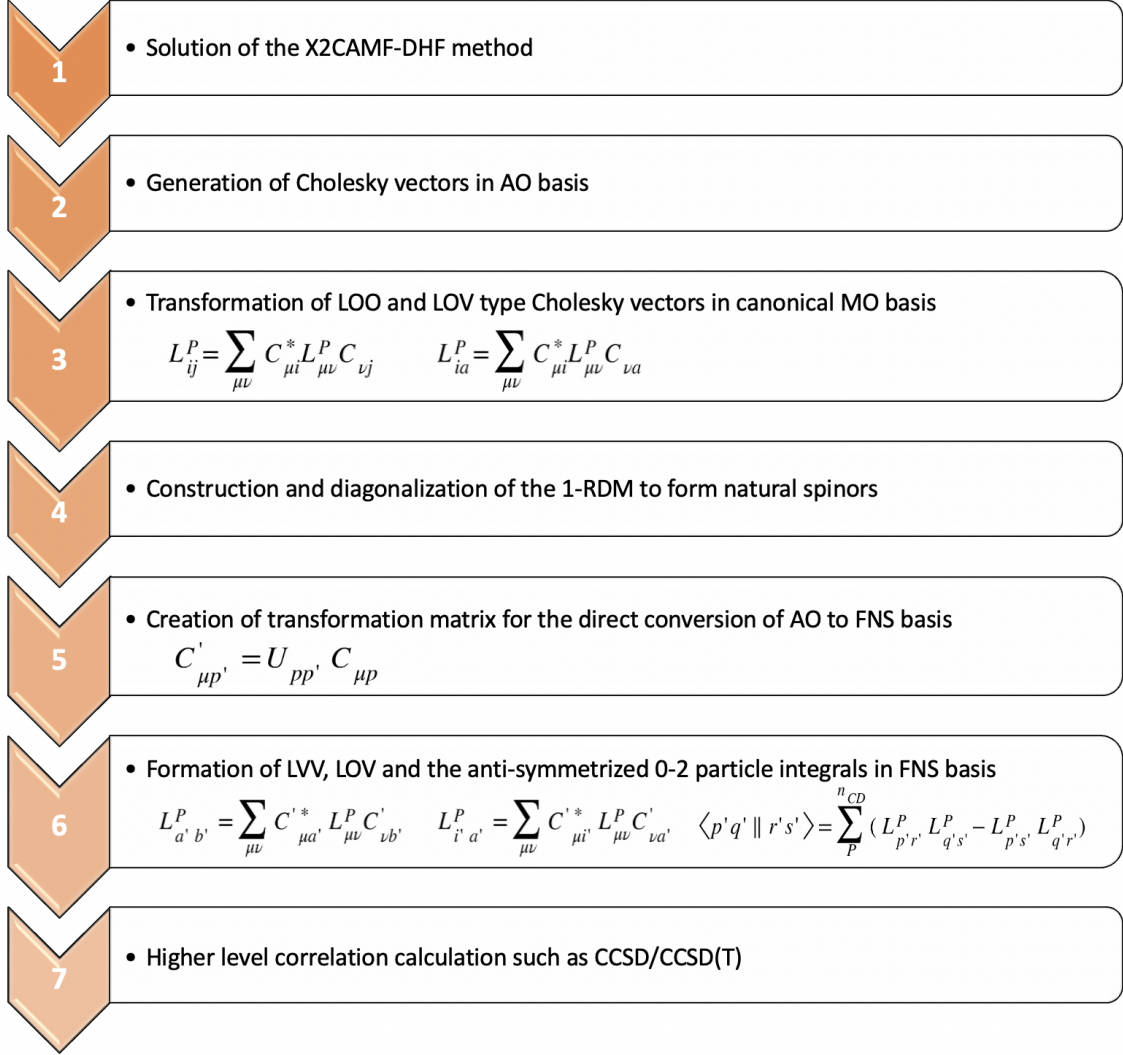


Figure 1: A schematic description of the FNS-CD-X2CAMF-CCSD/CCSD(T) algorithm.

prehensive analysis of the noncovalent dissociation enthalpies of ligands in 18 different complexes of coinage metal cations (Cu^+ , Ag^+ , and Au^+) in the gas phase for which credible experimental studies are available were carried out (See Figure 2). Optimized geometries for all the systems are taken from the work of Cavallo and coworkers.⁶⁹ For the ligands, the basis set employed was aug-cc-pVXZ (where X = D, T, and Q); on the other hand, for the metal cations (Cu^+ , Ag^+ , and Au^+), the basis set used was dyall.aexz (where x=2, 3, and 4). The basis sets were kept uncontracted, and the frozen core approximation was utilized for all the calculations. The gas phase noncovalent dissociation enthalpy (ΔH^0) of a ligand (L)

from a metal-ligand complex (ML_2) for a particular dissociation of type $ML_2 \rightarrow ML + L$ is calculated as:

$$\Delta H^0 = [E_0 + H_{corr}]_{ML} + [E_0 + H_{corr}]_L - [E_0 + H_{corr}]_{ML_2} \quad (40)$$

Where E_0 is the total electronic energy obtained after the solution of the FNS-CD-X2CAMF-CCSD/CCSD(T) method, and H_{corr} is the enthalpic correction added to the total electronic energy to determine the dissociation enthalpy. Our study will rely on the H_{corr} values provided in the work of Cavallo and coworkers⁶⁹ for different systems. By utilizing the basis extrapolation method, both the basis set superposition error (BSSE) and basis set incompleteness error (BSIE) can be evaded as with the extrapolation scheme; we move closer to the point of achieving a complete basis set (CBS) limit. In our current study, we employed the three-point extrapolation scheme proposed by Peterson and Dunning⁷⁰ to obtain the reference and correlation energy at the CBS limit. To calculate the dissociation enthalpy of a ligand from a metal-ligand complex at the CBS limit, we use Eq. (40) by plugging in the CBS limit values for DHF and correlation energies while keeping H_{corr} consistent with the previously reported value.⁶⁹

4 Results and discussion

4.1 Benchmark calculations for non-covalent bond dissociation enthalpy

Choosing suitable criteria to truncate the natural spinor virtual space holds the utmost significance. To ensure consistency across different atoms and molecules, the truncation framework should be uniformly applicable while also being seamlessly accessible as a black box. It has been well established in the literature the occupation of natural orbitals in the non-relativistic domain^{57,58} and natural spinors in the relativistic domain⁴⁰⁻⁴³ is a credible

criterion for arranging the natural orbitals/spinors in order of importance. Hence, in this particular study, we resort to the occupation number of natural spinors as a measure of criteria to truncate the virtual natural spinor space. By adjusting the predefined Cholesky threshold, one can optimize both storage demands and accuracy. To find the optimal threshold that balances computational efficiency with accuracy, we considered three truncation thresholds: LOOSEFNS (FNS threshold: 10^{-4} , and CD threshold: 10^{-3}), NORMALFNS (FNS threshold: $10^{-4.5}$, and CD threshold: 10^{-4}), and TIGHTFNS (FNS threshold: 10^{-5} , and CD threshold: 10^{-5}). We conducted CCSD and CCSD(T) calculations on 18 different metal-ligand complexes to determine which threshold is most appropriate for calculating non-covalent dissociation enthalpies. For the calculation, we chose the uncontracted aug-cc-pVDZ basis set for the ligands and the dyall.ae2z basis set for the metal. For each threshold, mean error (ME), mean absolute error (MAE), absolute maximum error (AME), and standard error (SE) were calculated. Cheng and co-workers³⁶ have shown that a Cholesky threshold of 10^{-5} gives very close results as that obtained using standard integrals version. We have also investigated the error introduced due to the Cholesky decomposition of integrals (See supporting information) and found the threshold of 10^{-5} gives nearly identical results as that of the X2CAMF-CC method with standard integrals. Therefore, the canonical CD-X2CAMF-CCSD/CCSD(T) results with full virtual space and Cholesky threshold of 10^{-5} were chosen as the reference. Table 1 shows the comparison of errors for CCSD and CCSD(T) methods for 18 metal-ligand complexes in three different thresholds. The error values are shown in Table 1. It can be seen that on moving from a LOOSEFNS to a NORMALFNS threshold, the error is significantly reduced in both the CCSD and CCSD(T) methods. The AME is reduced from 0.890 kcal/mol to 0.340 kcal/mol when going from LOOSEFNS to NORMALFNS. For the CCSD(T) method, the decrease in AME is 0.570 kcal/mol to 0.287 kcal/mol. The change from NORMALFNS to TIGHTFNS is comparatively smaller. The MAE observed in the FNS-CD-X2CAMF-CCSD(T) method with a TIGHTFNS threshold is 0.170 kcal/mol. The NORMALFNS makes a good compromise between computational cost and accuracy.

Therefore, the larger basis set calculations are performed using the NORMALFNS threshold only.

We have calculated the non-covalent bond dissociation enthalpies of ligands for the same 18 metal-ligand complexes in three different basis sets using the FNS-CD-X2CAMF-CCSD(T) method. The calculated energy values at aug-cc-pVDZ (dyall.ae2z for the metal), aug-cc-pVTZ (dyall.ae3z for the metal), and aug-cc-pVQZ (dyall.ae4z for the metal) level are extrapolated to obtain dissociation enthalpy at the CBS limit. The absolute values of the dissociation enthalpies in different bases are provided in Table S1. Figure 3 shows the enthalpy values in different basis sets calculated using the FNS-CD-X2CAMF-CCSD(T) method. The figure also includes the corresponding experimental values⁷¹⁻⁸² (with associated error bars) for comparison. From figure 3, it can be seen that dissociation enthalpy values at QZ and CBS limit are in good agreement with each other and less than 0.5 kcal/mol. The FNS-CD-X2CAMF-CCSD(T) results for a few complexes are a little off the experimental error bar. It is presumably due to the missing effect from higher-order excitation in the coupled cluster. Overall, we find the accuracy of the FNS-CD-X2CAMF-CCSD(T) method using normal threshold and at CBS limit to be reasonable in reproducing experimentally determined gas phase non-covalent dissociation enthalpies of ligands from coinage metal cation complexes.

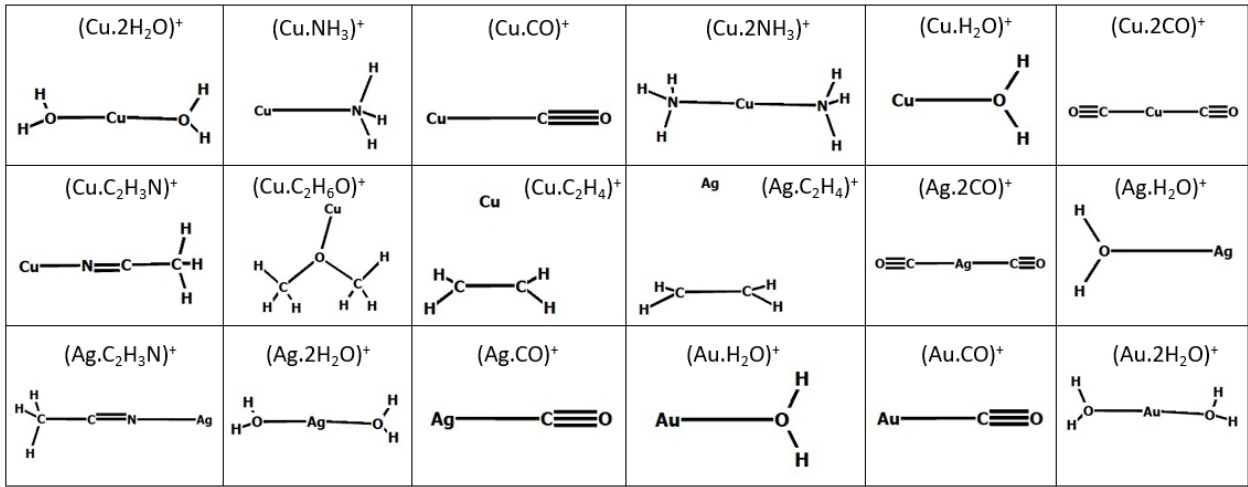


Figure 2: Molecular structures of the complexes used in the current work.

Table 1: Comparison of Mean Error (ME), Mean Absolute Error (MAE), Standard Error (SE), and Absolute Maximum Error (AME) (in kcal/mol) of FNS-CD-X2CAMF-CCSD and FNS-CD-X2CAMF-CCSD(T) methods with respect to their canonical values in the different truncation thresholds. The uncontracted aug-cc-pVDZ basis set is used for the ligands and the dyall.ae2z basis set is used for the metal.

Threshold	FNS-CD-X2CAMF-CCSD				FNS-CD-X2CAMF-CCSD(T)			
	ME	MAE	SE	AME	ME	MAE	SE	AME
LOOSEFNS	0.173	0.354	0.398	0.890	0.146	0.298	0.301	0.570
NORMALFNS	0.018	0.135	0.170	0.340	0.093	0.128	0.117	0.289
TIGHTFNS	0.021	0.107	0.135	0.250	0.000	0.071	0.091	0.170

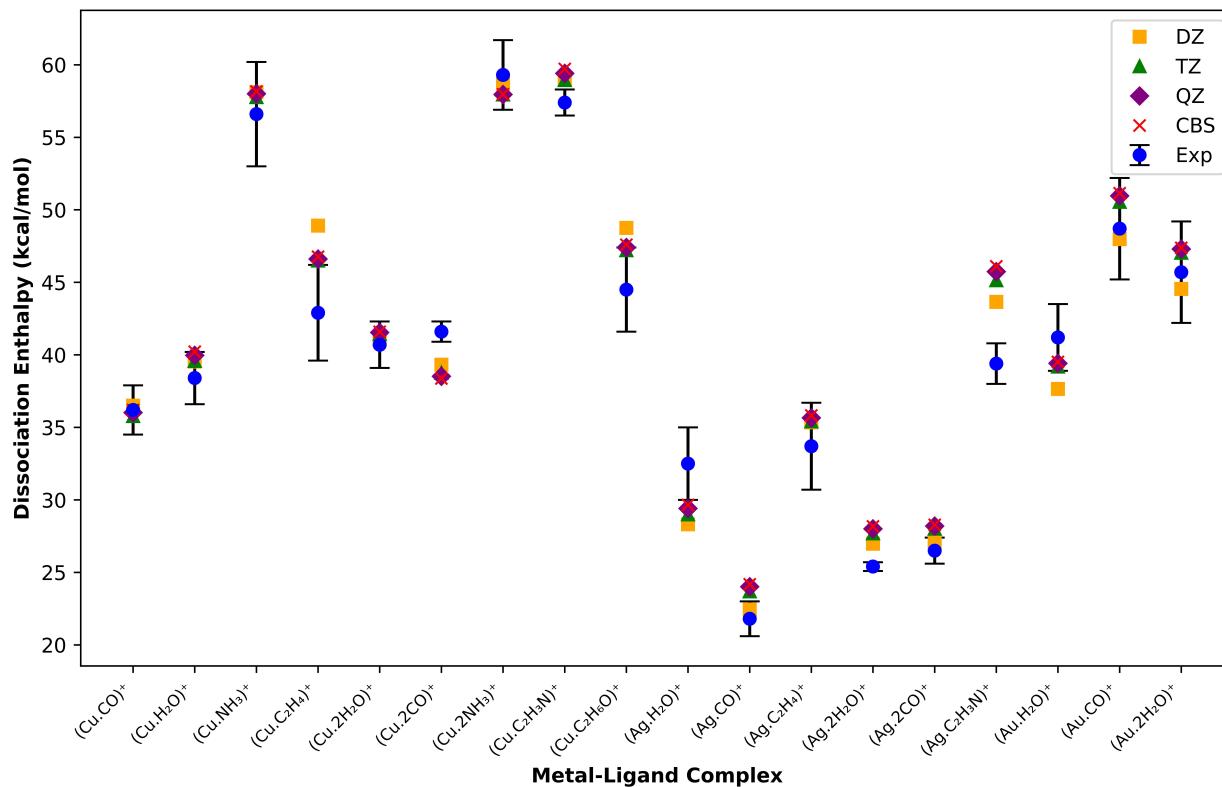


Figure 3: Experimental (with the error bars) and FNS-CD-X2CAMF-CCSD(T) bond dissociation enthalpies of ligand obtained for 18 different metal-ligand complexes at different basis sets.

4.2 Comparison with four-component FNS framework

To demonstrate the accuracy of the FNS-CD-X2CAMF method with respect to the four-component variant, we calculated the spectroscopic constants (bond length and harmonic vibrational frequency) for the hydrogen halide series (HX, X=F, Cl, Br, and I) using the FNS-CD-X2CAMF-CCSD and FNS-CD-X2CAMF-CCSD(T) methods. This energy derivative has been calculated through numerical differentiation of the total energy, utilizing the TWOFIT utility program in DIRAC software.⁸³ A fifth-degree polynomial was employed, and the basis set used was dyall.acv3z for the Br and I atoms and uncontracted aug-cc-pVTZ for the H, F, and Cl atoms. The same example was used to determine the accuracy of our original four-component FNS implementation.⁴⁰ Tables 2 and 3 display the errors in bond length and harmonic vibrational frequency for hydrogen halides relative to the canonical four-component values across three truncation thresholds. The tables also provide a comparison with the error values from the four-component FNS method. The canonical four-component values and FNS four-component error values are taken from our previous work.⁴⁰ All the error values presented in Tables 2 and 3 are perturbatively corrected for the FNS truncation. The FNS truncation used in ref⁴⁰ is 10^{-5} , which is the same as the TIGHTFNS setting in the present manuscript. Table 2 clearly shows that, with a tight threshold, the error values in the FNS-CD-X2CAMF-CCSD method are of a similar order of magnitude to those in the FNS-4c-CCSD method. This pattern is also observed in the FNS-CD-X2CAMF-CCSD(T) method. In our four-component-based implementation, we found that a threshold of 10^{-5} was adequate for obtaining converged results for the bond lengths of the hydrogen halide series. However, in the current implementation, we recommend using the NORMALFNS threshold as a truncation threshold, as it provides error values of a similar order of magnitude to those of a TIGHTFNS threshold while balancing accuracy and efficiency. Just like the bond lengths, the order of magnitude of the harmonic vibrational frequency error values at the TIGHTFNS threshold for the FNS-CD-X2CAMF-CCSD and

FNS-CD-X2CAMF-CCSD(T) methods is comparable to the error values from the FNS-4c-CCSD and FNS-4c-CCSD(T) methods, except the case in HI where the FNS-CD-X2CAMF variant works little better. The harmonic frequency results for all molecules in the FNS-4c-CCSD and FNS-4c-CCSD(T) methods are within 10 cm^{-1} of their canonical counterparts. While the error in bond lengths for the LOOSEFNS threshold was not significant, it is more pronounced for the harmonic frequency values. The maximum deviation of the harmonic frequency values from the canonical 4c method exceeds 11 cm^{-1} . The NORMALFNS threshold gives an economic compromise with error within 5 cm^{-1} of the canonical 4c values,

Table 2: Comparison of error in bond length (in Å), with respect to the canonical four-component values (4c) in the different truncation thresholds. The basis set used was dyall.acv3z for the Br and I atoms and uncontracted aug-cc-pVTZ for the H, F, and Cl atoms.

Molecule	CCSD					CCSD(T)				
	4c	FNS-4c	FNS-CD-X2CAMF			4c	FNS-4c	FNS-CD-X2CAMF		
			LOOSE	NORMAL	TIGHT			LOOSE	NORMAL	TIGHT
HF	0.9183	0.0000	0.0008	0.0003	0.0001	0.9213	0.0000	0.0002	0.0002	-0.0001
HCl	1.2753	0.0000	0.0002	0.0000	-0.0001	1.2777	0.0000	0.0002	-0.0001	-0.0001
HBr	1.4089	0.0005	0.0004	0.0004	0.0001	1.4117	0.0003	0.0002	0.0002	0.0000
HI	1.6027	0.0004	0.0009	0.0005	0.0003	1.6059	0.0004	0.0011	0.0004	0.0002

Table 3: Comparison of error in harmonic vibrational frequency (in cm^{-1}), with respect to the canonical four-component values (4c) in the different truncation thresholds. The basis set used was dyall.acv3z for the Br and I atoms and uncontracted aug-cc-pVTZ for the H, F, and Cl atoms.

Molecule	CCSD					CCSD(T)				
	4c	FNS-4c	FNS-CD-X2CAMF			4c	FNS-4c	FNS-CD-X2CAMF		
			LOOSE	NORMAL	TIGHT			LOOSE	NORMAL	TIGHT
HF	4083.08	-0.08	-11.7	-4.54	0.07	4036.44	1.06	-3.6	-3.22	1.18
HCl	3015.13	-0.03	-3.06	0.41	-0.02	2990.66	0.24	-3.25	1.23	0.21
HBr	2673.1	-0.63	-0.64	-3.08	-0.97	2647.42	-0.03	1.24	-0.82	-0.4
HI	2333.7	-9.09	-10.32	-3.39	-2.32	2306.75	-7.59	-8.41	-1.96	-2.71

4.3 Computational efficiency

To compare the computational efficiency between the four-component canonical CCSD (4c), four-component FNS-CCSD (FNS-4c), and the FNS-CD-X2CAMF-CCSD method, we have calculated the CCSD energy for the HI molecule. An uncontracted aug-cc-pVTZ basis set for H atom and dyall.acv3z basis set for the I atom was used for the calculations. The calculations were carried out sequentially on a dedicated workstation with two Intel(R) Xeon(R) Gold 5315Y processors @ 3.20 GHz. The workstation had a total of 512 GB of RAM. The core electrons were kept frozen throughout the correlation calculation. An FNS threshold of 10^{-5} and a tight threshold (FNS threshold: 10^{-5} , and CD threshold: 10^{-5}) were used for FNS-4c and FNS-CD-X2CAMF CCSD calculations. The virtual space consists of 434 virtuals in the canonical spinor basis. However, in the truncated frozen natural spinor basis, this dimension decreases significantly to 174. Table 4 indicates the storage demand of all the MO integrals involving virtual indices and the time taken for their formation in the four-component canonical spinor basis, four-component FNS basis, and CD-X2CAMF based two-component FNS basis. It is clear from the table 4 that a large computational saving in terms of storage can be achieved by using the FNS-CD-X2CAMF scheme, as it avoids the formation/storage of four and three virtual type integrals and leading to the reduction in timing. In the present implementation, the integrals with two-virtual or one-virtual indices have similar storage requirements in FNS-4c and FNS-CD-X2CAMF methods. However, the time required to construct them is much smaller in the FNS-CD-X2CAMF method. Figure 4 displays the timings for integral formation, CCSD iteration, and the total time taken in the calculation of the HI molecule. The FNS-based implementation for 4c-CCSD takes just a fraction of the timing for MO integral formation and the CCSD iterations and hence leads to a drastic reduction in the computational cost. The FNS-CD-X2CAMF-CCSD scheme takes almost the same time for the CCSD iterations as the FNS-4c-CCSD method. However, the time required for integral construction in the FNS basis is negligible in the former, which

greatly reduces the overall timing. The FNS-CD-X2CAMF-CCSD calculations are ~ 11 times faster than the four-component FNS-CCSD calculation and are ~ 38 times faster than the four-component canonical CCSD calculations, meanwhile lifting the storage bottlenecks as well.

Table 4: Size of the integral used, and time taken to compute them in canonical four-component (4c), FNS four-component (FNS-4c), and FNS-CD-X2CAMF two-component method for HI molecule. The basis set used was dyall.acv3z for the I atom and uncontracted aug-cc-pVTZ for the H atom.

Integral	Storage (GB)			Time taken (seconds)		
	4c	FNS-4c	FNS-CD-X2CAMF	4c	FNS-4c	FNS-CD-X2CAMF
VVVV	2150	55	-	13407	1626	-
OVVV	110	7	-	1212	812	-
OOVV	0.9	0.14	0.14	659	610	0.35
OOOV	0.19	0.07	0.07	865	782	0.06

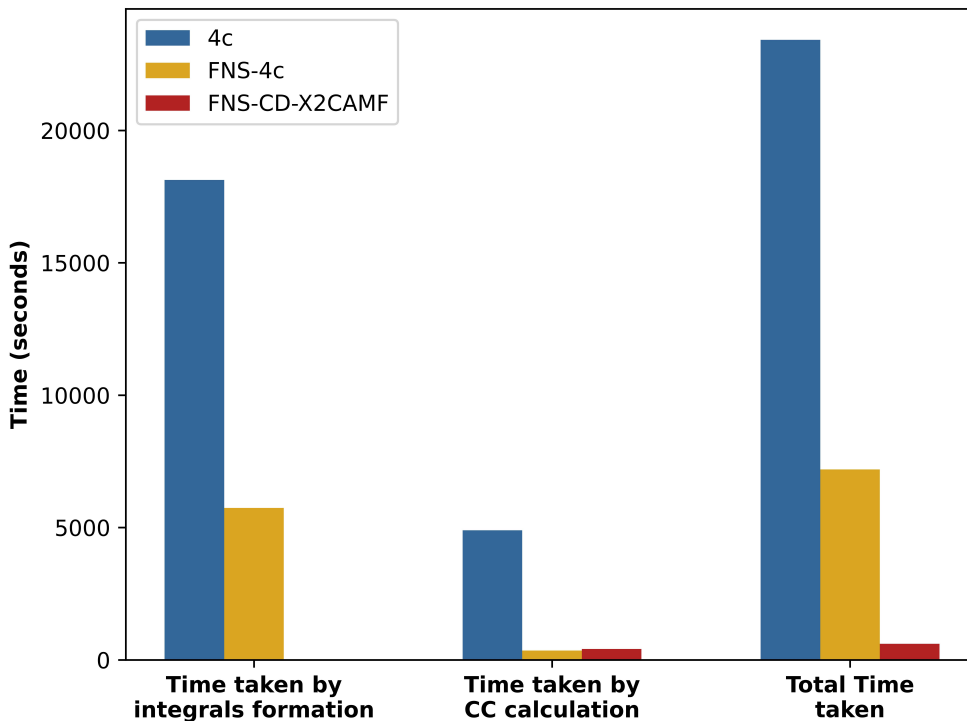


Figure 4: Comparison of the time taken by the different steps in correlation calculation of HI molecule in canonical four-component (4c), FNS four-component (FNS-4c), and FNS-CD-X2CAMF two-component method. The basis set used was dyall.acv3z for the I atom and uncontracted aug-cc-pVTZ for the H atom.

4.4 Application to medium-sized complex

As a potential application of the FNS-CD-X2CAMF-CCSD method, we performed correlation calculation for $[\text{UO}_2(\text{NO}_3)_3]^-$ complex. The geometry for the complex is taken from the work of Pototschnig and co-workers.³⁷ The molecular structure of the complex is shown in Figure 5. An uncontracted aug-cc-pVDZ basis set for H, O, and N atom and s-aug-dyall.v2z basis set for the U atom was used for the calculations. The $[\text{UO}_2(\text{NO}_3)_3]^-$ complex has a basis set of dimension 1594 with 202 occupied spinors and 1392 virtual spinors. The core electrons were kept frozen through the correlation calculation, and a LOOSEFNS truncation threshold was used for the FNS-CD-X2CAMF-CCSD calculation, resulting in 106 occupied spinors and 562 virtual spinors. The number of Cholesky vectors at the loose threshold is

2441. The calculations were carried out sequentially on a specialized workstation equipped with two Intel(R) Xeon(R) Gold 5315Y processors @ 3.20 GHz and a total of 2.0 TB of RAM. The time taken in Cholesky vector formation in the AO basis is 17 minutes and 17 seconds. Since the OOVV type integrals in a canonical basis also possess a storage bottleneck for this case, they are also generated on the fly and are directly stored on the memory in the FNS basis. The time taken by the two-electron integral formations in the FNS basis is 8 minutes and 16 seconds. The CCSD calculation took 2 days, 5 hours, 59 minutes, and 10 seconds. Out of which, 16 hours are taken by the construction of the particle-particle ladder term ($\sum_{ef} \langle ab || ef \rangle t_{ef}^{ij}$).

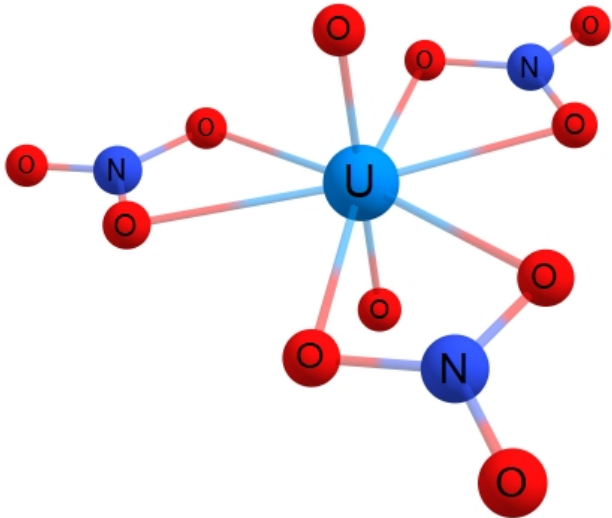


Figure 5: Molecular structure for the $[\text{UO}_2(\text{NO}_3)_3]^-$ complex.

5 Conclusions

In this study, we propose an efficient FNS-CD-X2CAMF-CCSD/CCSD(T) method that incorporates frozen natural spinors and the Cholesky decomposition technique for two-component X2CAMF-CCSD/CCSD(T) methods. Our benchmark calculations on gas phase non-covalent ligand dissociation enthalpy of coinage metal ion complexes demonstrate that a normal threshold is sufficient to achieve a balanced trade-off between maintaining chemi-

cal accuracy and computational efficiency. The ability of the FNS-CD-X2CAMF-CCSD(T) method to accurately replicate the experimental gas-phase non-covalent ligand dissociation enthalpy at the CBS limit has been investigated, and our calculation shows that a reasonable level of accuracy for calculating bond dissociation enthalpies can be achieved. The comparison between the computational efficiency of the CCSD calculations using four-component canonical, four-component FNS, and two-component FNS-CD-X2CAMF methods demonstrates that FNS-CD-X2CAMF-based relativistic calculations are significantly faster than their canonical four-component counterparts as well as outrank them in terms of storage requirement of two-electron integrals. The FNS-CD-X2CAMF framework leads to a significant reduction in the computation cost of the coupled cluster method over the standard 4c-FNS framework both in terms of storage requirements and computational time which can significantly reduce the computational cost. The method's applicability was further supported by a correlation calculation for a medium-sized uranium complex. It shows that the method can be routinely used for accurate relativistic calculations of small molecules, even with modest computational resources. A massively parallel version of the FNS-CD-X2CAMF-CCSD/CCSD(T) method will lead to its widespread adoption, in computational studies related to heavy element-containing systems and complexes. Work is in progress in that direction.

Acknowledgement

The authors acknowledge the support from the IIT Bombay, CRG, and Matrix project of DST-SERB, CSIR-India, DST-Inspire Faculty Fellowship, Prime Minister's Research Fellowship, ISRO for financial support, IIT Bombay super computational facility, and C-DAC Super- computing resources (PARAM Yuva-II, Param Bramha) for computational time.

Supporting Information Available

The following file is available free of charge.

- SI: The convergence of the FNS-CD-X2CAMF-CCSD and CCSD(T) bond dissociation enthalpies with respect to the Cholesky threshold and the absolute values of the dissociation enthalpies in different bases.

References

- (1) Eliav, E.; Kaldor, U.; Ishikawa, Y. Open-shell relativistic coupled-cluster method with Dirac-Fock-Breit wave functions: Energies of the gold atom and its cation. *Phys. Rev. A* **1994**, *49*, 1724–1729.
- (2) Eliav, E.; Kaldor, U.; Ishikawa, Y. Relativistic coupled cluster theory based on the no-pair dirac-coulomb-breit hamiltonian: Relativistic pair correlation energies of the xe atom. *Int. J. Quantum Chem.* **1994**, *52*, 205–214.
- (3) Visscher, L.; Dyall, K. G.; Lee, T. J. Kramers-restricted closed-shell CCSD theory. *Int. J. Quantum Chem.* **1995**, *56*, 411–419.
- (4) Visscher, L.; Lee, T. J.; Dyall, K. G. Formulation and implementation of a relativistic unrestricted coupled-cluster method including noniterative connected triples. *J. Chem. Phys.* **1996**, *105*, 8769–8776.
- (5) Lee, H.-S.; Han, Y.-K.; Kim, M. C.; Bae, C.; Lee, Y. S. Spin-orbit effects calculated by two-component coupled-cluster methods: test calculations on AuH, Au₂, TlH and Tl₂. *Chem. Phys. Lett.* **1998**, *293*, 97–102.
- (6) Nataraj, H. S.; Kállay, M.; Visscher, L. General implementation of the relativistic coupled-cluster method. *J. Chem. Phys.* **2010**, *133*, 234109.

- (7) Liu, J.; Cheng, L. Relativistic coupled-cluster and equation-of-motion coupled-cluster methods. *WIREs Comput. Mol. Sci.* **2021**, *11*, e1536.
- (8) Hess, B. A. Relativistic electronic-structure calculations employing a two-component no-pair formalism with external-field projection operators. *Phys. Rev. A* **1986**, *33*, 3742–3748.
- (9) van Lenthe, E.; van Leeuwen, R.; Baerends, E. J.; Snijders, J. G. Relativistic regular two-component Hamiltonians. *Int. J. Quantum Chem.* **1996**, *57*, 281–293.
- (10) Dyall, K. G. Interfacing relativistic and nonrelativistic methods. I. Normalized elimination of the small component in the modified Dirac equation. *J. Chem. Phys.* **1997**, *106*, 9618–9626.
- (11) Nakajima, T.; Hirao, K. A new relativistic theory: a relativistic scheme by eliminating small components (RESC). *Chem. Phys. Lett.* **1999**, *302*, 383–391.
- (12) Barysz, M.; Sadlej, A. J. Two-component methods of relativistic quantum chemistry: from the Douglas-Kroll approximation to the exact two-component formalism. *J. Mol. Struct.: THEOCHEM* **2001**, *573*, 181–200.
- (13) Liu, W.; Peng, D. Exact two-component Hamiltonians revisited. *J. Chem. Phys.* **2009**, *131*, 031104.
- (14) Saue, T. Relativistic Hamiltonians for Chemistry : A Primer. *ChemPhysChem* **2011**, *12*, 3077–3094.
- (15) Kutzelnigg, W.; Liu, W. Quasirelativistic theory equivalent to fully relativistic theory. *J. Chem. Phys.* **2005**, *123*, 241102.
- (16) Iliáš, M.; Saue, T. An infinite-order two-component relativistic Hamiltonian by a simple one-step transformation. *J. Chem. Phys.* **2007**, *126*, 064102.

- (17) Dyall, K. G.; Faegri, K. *Introduction to Relativistic Quantum Chemistry*; Oxford University Press, 2007.
- (18) Kirsch, T.; Engel, F.; Gauss, J. Analytic evaluation of first-order properties within the mean-field variant of spin-free exact two-component theory. *J. Chem. Phys.* **2019**, *150*, 204115.
- (19) Zou, W.; Filatov, M.; Cremer, D. Development and application of the analytical energy gradient for the normalized elimination of the small component method. *J. Chem. Phys.* **2011**, *134*, 244117.
- (20) Filatov, M.; Zou, W.; Cremer, D. Calculation of response properties with the normalized elimination of the small component method. *Int. J. Quantum Chem.* **2014**, *114*, 993–1005.
- (21) Cheng, L.; Gauss, J. Analytic energy gradients for the spin-free exact two-component theory using an exact block diagonalization for the one-electron Dirac Hamiltonian. *J. Chem. Phys.* **2011**, *135*, 084114.
- (22) Sikkema, J.; Visscher, L.; Saue, T.; Iliáš, M. The molecular mean-field approach for correlated relativistic calculations. *J. Chem. Phys.* **2009**, *131*, 124116.
- (23) Tecmer, P.; Severo Pereira Gomes, A.; Knecht, S.; Visscher, L. Communication: Relativistic Fock-space coupled cluster study of small building blocks of larger uranium complexes. *J. Chem. Phys.* **2014**, *141*, 041107.
- (24) Pototschnig, J. V.; Papadopoulos, A.; Lyakh, D. I.; Repisky, M.; Halbert, L.; Severo Pereira Gomes, A.; Jensen, H. J. A.; Visscher, L. Implementation of Relativistic Coupled Cluster Theory for Massively Parallel GPU-Accelerated Computing Architectures. *J. Chem. Theory Comput.* **2021**, *17*, 5509–5529, PMID: 34370471.

- (25) Iliáš, M.; Kellö, V.; Visscher, L.; Schimmelpfennig, B. Inclusion of mean-field spin-orbit effects based on all-electron two-component spinors: Pilot calculations on atomic and molecular properties. *J. Chem. Phys.* **2001**, *115*, 9667–9674.
- (26) Zhang, T.; Banerjee, S.; Koulias, L. N.; Valeev, E. F.; DePrince, A. E. I.; Li, X. Dirac-Coulomb-Breit Molecular Mean-Field Exact-Two-Component Relativistic Equation-of-Motion Coupled-Cluster Theory. *J. Phys. Chem. A* **2024**, *128*, 3408–3418, PMID: 38651293.
- (27) Heß, B. A.; Marian, C. M.; Wahlgren, U.; Gropen, O. A mean-field spin-orbit method applicable to correlated wavefunctions. *Chem. Phys. Lett.* **1996**, *251*, 365–371.
- (28) Liu, J.; Cheng, L. An atomic mean-field spin-orbit approach within exact two-component theory for a non-perturbative treatment of spin-orbit coupling. *J. Chem. Phys.* **2018**, *148*, 144108.
- (29) Zhang, C.; Cheng, L. Atomic Mean-Field Approach within Exact Two-Component Theory Based on the Dirac-Coulomb-Breit Hamiltonian. *J. Phys. Chem. A* **2022**, *126*, 4537–4553, PMID: 35763592.
- (30) Knecht, S.; Repisky, M.; Jensen, H. J. A.; Saue, T. Exact two-component Hamiltonians for relativistic quantum chemistry: Two-electron picture-change corrections made simple. *J. Chem. Phys.* **2022**, *157*, 114106.
- (31) Kelley, M. S.; Shiozaki, T. Large-scale Dirac-Fock-Breit method using density fitting and 2-spinor basis functions. *J. Chem. Phys.* **2013**, *138*, 204113.
- (32) Bates, J. E.; Shiozaki, T. Fully relativistic complete active space self-consistent field for large molecules: Quasi-second-order minimax optimization. *J. Chem. Phys.* **2015**, *142*, 044112.

- (33) Helmich-Paris, B.; Repisky, M.; Visscher, L. Relativistic Cholesky-decomposed density matrix MP2. *Chem. Phys.* **2019**, *518*, 38–46.
- (34) Banerjee, S.; Zhang, T.; Dylla, K. G.; Li, X. Relativistic resolution-of-the-identity with Cholesky integral decomposition. *J. Chem. Phys.* **2023**, *159*, 114119.
- (35) Uhlřřova, T.; Cianchino, D.; Nottoli, T.; Lipparini, F.; Gauss, J. Cholesky Decomposition in Spin-Free Dirac-Coulomb Coupled-Cluster Calculations. *J. Phys. Chem. A* **2024**, *128*, 8292–8303, PMID: 39268870.
- (36) Zhang, C.; Lipparini, F.; Stopkowicz, S.; Gauss, J.; Cheng, L. Cholesky Decomposition-Based Implementation of Relativistic Two-Component Coupled-Cluster Methods for Medium-Sized Molecules. *J. Chem. Theory Comput.* **2024**, *20*, 787–798, PMID: 38198515.
- (37) Ufimtsev, I. S.; Martınez, T. J. Quantum Chemistry on Graphical Processing Units. 1. Strategies for Two-Electron Integral Evaluation. *J. Chem. Theory Comput.* **2008**, *4*, 222–231, PMID: 26620654.
- (38) DePrince, A. E. I.; Hammond, J. R. Coupled Cluster Theory on Graphics Processing Units I. The Coupled Cluster Doubles Method. *J. Chem. Theory Comput.* **2011**, *7*, 1287–1295, PMID: 26610123.
- (39) Lowdin, P.-O. Quantum Theory of Many-Particle Systems. I. Physical Interpretations by Means of Density Matrices, Natural Spin-Orbitals, and Convergence Problems in the Method of Configurational Interaction. *Phys. Rev.* **1955**, *97*, 1474–1489.
- (40) Chamoli, S.; Surjuse, K.; Jangid, B.; Nayak, M. K.; Dutta, A. K. A reduced cost four-component relativistic coupled cluster method based on natural spinors. *J. Chem. Phys.* **2022**, *156*, 204120.

- (41) Surjuse, K.; Chamoli, S.; Nayak, M. K.; Dutta, A. K. A low-cost four-component relativistic equation of motion coupled cluster method based on frozen natural spinors: Theory, implementation, and benchmark. *J. Chem. Phys.* **2022**, *157*, 204106.
- (42) Chamoli, S.; Nayak, M. K.; Dutta, A. K. In *Electron Density*; Chattaraj, P. K., Chakraborty, D., Eds.; John Wiley & Sons Ltd, 2024; Chapter 5.
- (43) Yuan, X.; Visscher, L.; Gomes, A. S. P. Assessing MP2 frozen natural orbitals in relativistic correlated electronic structure calculations. *J. Chem. Phys.* **2022**, *156*, 224108.
- (44) Sucher, J. Foundations of the relativistic theory of many-electron atoms. *Phys. Rev. A* **1980**, *22*, 348–362.
- (45) Dyall, K. G. An exact separation of the spin-free and spin-dependent terms of the Dirac-Coulomb-Breit Hamiltonian. *J. Chem. Phys.* **1994**, *100*, 2118–2127.
- (46) Shavitt, I.; Bartlett, R. J. *Many-Body Methods in Chemistry and Physics: MBPT and Coupled-Cluster Theory*; Cambridge Molecular Science; Cambridge University Press, 2009.
- (47) Beebe, N. H. F.; Linderberg, J. Simplifications in the generation and transformation of two-electron integrals in molecular calculations. *Int. J. Quantum Chem.* **1977**, *12*, 683–705.
- (48) Zeng, T.; Fedorov, D. G.; Schmidt, M. W.; Klobukowski, M. Two-component natural spinors from two-step spin-orbit coupled wave functions. *J. Chem. Phys.* **2011**, *134*, 214107.
- (49) Zeng, T.; Fedorov, D. G.; Schmidt, M. W.; Klobukowski, M. Effects of Spin-Orbit Coupling on Covalent Bonding and the Jahn-Teller Effect Are Revealed with the Natural Language of Spinors. *J. Chem. Theory Comput.* **2011**, *7*, 2864–2875, PMID: 26605477.

- (50) Zeng, T.; Fedorov, D. G.; Schmidt, M. W.; Klobukowski, M. Natural Spinors Reveal How the Spin-Orbit Coupling Affects the Jahn-Teller Distortions in the Hexafluorotungstate(V) Anion. *J. Chem. Theory Comput.* **2012**, *8*, 3061–3071, PMID: 26605717.
- (51) Edmiston, C.; Krauss, M. Configuration-Interaction Calculation of H₃ and H₂. *J. Chem. Phys.* **1965**, *42*, 1119–1120.
- (52) Ahlrichs, R.; Kutzelnigg, W. Direct Calculation of Approximate Natural Orbitals and Natural Expansion Coefficients of Atomic and Molecular Electronic Wavefunctions. II. Decoupling of the Pair Equations and Calculation of the Pair Correlation Energies for the Be and LiH Ground States. *J. Chem. Phys.* **1968**, *48*, 1819–1832.
- (53) Barr, T. L.; Davidson, E. R. Nature of the Configuration-Interaction Method in Ab Initio Calculations. I. Ne Ground State. *Phys. Rev. A* **1970**, *1*, 644–658.
- (54) Jensen, H. J. A.; Jørgensen, P.; Ågren, H.; Olsen, J. Second-order Møller-Plesset perturbation theory as a configuration and orbital generator in multiconfiguration self-consistent field calculations. *J. Chem. Phys.* **1988**, *88*, 3834–3839.
- (55) Taube, A. G.; Bartlett, R. J. Frozen natural orbitals: systematic basis set truncation for coupled-cluster theory. *Collect. Czech. Chem. Commun.* **2005**, *70*, 837–850.
- (56) Neese, F.; Wennmohs, F.; Hansen, A. Efficient and accurate local approximations to coupled-electron pair approaches: An attempt to revive the pair natural orbital method. *J. Chem. Phys.* **2009**, *130*, 114108.
- (57) Neese, F.; Hansen, A.; Liakos, D. G. Efficient and accurate approximations to the local coupled cluster singles doubles method using a truncated pair natural orbital basis. *J. Chem. Phys.* **2009**, *131*, 064103.
- (58) Landau, A.; Khistyayev, K.; Dolgikh, S.; Krylov, A. I. Frozen natural orbitals for ionized

- states within equation-of-motion coupled-cluster formalism. *J. Chem. Phys.* **2010**, *132*, 014109.
- (59) Mata, R. A.; Stoll, H. An incremental correlation approach to excited state energies based on natural transition/localized orbitals. *J. Chem. Phys.* **2011**, *134*, 034122.
- (60) Kumar, A.; Crawford, T. D. Frozen Virtual Natural Orbitals for Coupled-Cluster Linear-Response Theory. *J. Phys. Chem. A* **2017**, *121*, 708–716, PMID: 28045265.
- (61) Mester, D.; Nagy, P. R.; Kállay, M. Reduced-cost linear-response CC2 method based on natural orbitals and natural auxiliary functions. *J. Chem. Phys.* **2017**, *146*, 194102.
- (62) Schwilk, M.; Ma, Q.; Köppl, C.; Werner, H.-J. Scalable Electron Correlation Methods. 3. Efficient and Accurate Parallel Local Coupled Cluster with Pair Natural Orbitals (PNO-LCCSD). *J. Chem. Theory Comput.* **2017**, *13*, 3650–3675, PMID: 28661673.
- (63) Nagy, P. R.; Samu, G.; Kállay, M. Optimization of the Linear-Scaling Local Natural Orbital CCSD(T) Method: Improved Algorithm and Benchmark Applications. *J. Chem. Theory Comput.* **2018**, *14*, 4193–4215, PMID: 29965753.
- (64) Pokhilko, P.; Izmodenov, D.; Krylov, A. I. Extension of frozen natural orbital approximation to open-shell references: Theory, implementation, and application to single-molecule magnets. *J. Chem. Phys.* **2020**, *152*, 034105.
- (65) Folkestad, S. D.; Koch, H. Multilevel CC2 and CCSD Methods with Correlated Natural Transition Orbitals. *J. Chem. Theory Comput.* **2020**, *16*, 179–189, PMID: 31743013.
- (66) Gyevi-Nagy, L.; Kállay, M.; Nagy, P. R. Accurate Reduced-Cost CCSD(T) Energies: Parallel Implementation, Benchmarks, and Large-Scale Applications. *J. Chem. Theory Comput.* **2021**, *17*, 860–878, PMID: 33400527.
- (67) Dutta, A. K.; Manna, A.; Jangid, B.; Majee, K.; Surjuse, K.; Mukherjee, M.; Thapa, M.; Arora, S.; Chamoli, S.; Halder, S.; Chakraborty, S.; Mukhopadhyay, T. BAGH: A

- Quantum Chemistry Software Package. 2023; <https://sites.google.com/iitb.ac.in/bagh>, Accessed: 2023-09-19.
- (68) Xubwa socutils. 2024; <https://github.com/xubwa/socutils>, Accessed: 2024-12-24.
- (69) Minenkov, Y.; Chermak, E.; Cavallo, L. Accuracy of DLPNO-CCSD(T) Method for Noncovalent Bond Dissociation Enthalpies from Coinage Metal Cation Complexes. *J. Chem. Theory Comput.* **2015**, *11*, 4664–4676, PMID: 26574257.
- (70) Peterson, K. A.; Woon, D. E.; Dunning, J., Thom H. Benchmark calculations with correlated molecular wave functions. IV. The classical barrier height of the $\text{H} + \text{H}_2 \rightarrow \text{H}_2 + \text{H}$ reaction. *J. Chem. Phys.* **1994**, *100*, 7410–7415.
- (71) Meyer, F.; Chen, Y.-M.; Armentrout, P. B. Sequential Bond Energies of $\text{Cu}(\text{CO})_x^+$ and $\text{Ag}(\text{CO})_x^+$ ($x = 1-4$). *J. Am. Chem. Soc.* **1995**, *117*, 4071–4081.
- (72) Dalleska, N. F.; Honma, K.; Sunderlin, L. S.; Armentrout, P. B. Solvation of Transition Metal Ions by Water. Sequential Binding Energies of $\text{M}^+(\text{H}_2\text{O})_x$ ($x = 1-4$) for $\text{M} = \text{Ti}$ to Cu Determined by Collision-Induced Dissociation. *J. Am. Chem. Soc.* **1994**, *116*, 3519–3528.
- (73) Walter, D.; Armentrout, P. B. Sequential Bond Dissociation Energies of $\text{M}^+(\text{NH}_3)_x$ ($x = 1-4$) for $\text{M} = \text{Ti-Cu}$. *J. Am. Chem. Soc.* **1998**, *120*, 3176–3187.
- (74) Sievers, M. R.; Jarvis, L. M.; Armentrout, P. B. Transition-Metal Ethene Bonds: Thermochemistry of $\text{M}^+(\text{C}_2\text{H}_4)_n$ ($\text{M} = \text{Ti-Cu}$, $n = 1$ and 2) Complexes. *J. Am. Chem. Soc.* **1998**, *120*, 1891–1899.
- (75) Vitale, G.; Valina, A. B.; Huang, H.; Amunugama, R.; Rodgers, M. T. Solvation of Copper Ions by Acetonitrile. Structures and Sequential Binding Energies of $\text{Cu}^+(\text{CH}_3\text{CN})_x$, $x = 1-5$, from Collision-Induced Dissociation and Theoretical Studies. *J. Phys. Chem. A* **2001**, *105*, 11351–11364.

- (76) Koizumi, H.; Zhang, X.-G.; Armentrout, P. B. Collision-Induced Dissociation and Theoretical Studies of Cu^+ -Dimethyl Ether Complexes. *J. Phys. Chem. A* **2001**, *105*, 2444–2452.
- (77) El Aribi, H.; Shoeib, T.; Ling, Y.; Rodriguez, C. F.; Hopkinson, A. C.; Siu, K. W. M. Binding Energies of the Silver Ion to Small Oxygen-Containing Ligands: Determination by Means of Density Functional Theory and Threshold Collision-Induced Dissociation. *J. Phys. Chem. A* **2002**, *106*, 2908–2914.
- (78) Guo, B.; Castleman, A. The bonding strength of $\text{Ag}^+(\text{C}_2\text{H}_4)$ and $\text{Ag}^+(\text{C}_2\text{H}_4)_2$ complexes. *Chem. Phys. Lett.* **1991**, *181*, 16–20.
- (79) Holland, P. M.; Castleman, J., A. W. The thermochemical properties of gas-phase transition metal ion complexes. *J. Chem. Phys.* **1982**, *76*, 4195–4205.
- (80) Shoeib, T.; El Aribi, H.; Siu, K. W. M.; Hopkinson, A. C. A Study of Silver (I) Ion-Organonitrile Complexes: Ion Structures, Binding Energies, and Substituent Effects. *J. Phys. Chem. A* **2001**, *105*, 710–719.
- (81) Poisson, L.; Lepetit, F.; Mestdagh, J.-M.; Visticot, J.-P. Multifragmentation of the $\text{Au}(\text{H}_2\text{O})_{n \leq 10}^+$ Cluster Ions by Collision with Helium. *J. Phys. Chem. A* **2002**, *106*, 5455–5462.
- (82) Schwarz, H. Relativistic Effects in Gas-Phase Ion Chemistry: An Experimentalist's View. *Angew. Chem., Int. Ed.* **2003**, *42*, 4442–4454.
- (83) DIRAC, a relativistic ab initio electronic structure program, Release DIRAC22 (2022), written by H. J. Aa. Jensen, R. Bast, A. S. P. Gomes, T. Saue and L. Visscher, with contributions from I. A. Aucar, V. Bakken, C. Chibueze, J. Creutzberg, K. G. Dyall, S. Dubillard, U. Ekström, E. Eliav, T. Enevoldsen, E. Faßhauer, T. Fleig, O. Fossgaard, L. Halbert, E. D. Hedegård, T. Helgaker, B. Helmich–Paris, J. Henriksson,

M. van Horn, M. Iliáš, Ch. R. Jacob, S. Knecht, S. Komorovský, O. Kullie, J. K. Lærdahl, C. V. Larsen, Y. S. Lee, N. H. List, H. S. Nataraj, M. K. Nayak, P. Norman, G. Olejniczak, J. Olsen, J. M. H. Olsen, A. Papadopoulos, Y. C. Park, J. K. Pedersen, M. Pernpointner, J. V. Pototschnig, R. di Remigio, M. Repisky, K. Ruud, P. Sałek, B. Schimmelfennig, B. Senjean, A. Shee, J. Sikkema, A. Sunaga, A. J. Thorvaldsen, J. Thyssen, J. van Stralen, M. L. Vidal, S. Villaume, O. Visser, T. Winther, S. Yamamoto and X. Yuan (available at <http://dx.doi.org/10.5281/zenodo.6010450>, see also <http://www.diracprogram.org>).